Paper # 070CO-0312 Topic: Coal and biomass combustion and gasification

8th US National Combustion Meeting
Organized by the Western States Section of the Combustion Institute
and hosted by the University of Utah
May 19-22, 2013.

Transient simulations of char gasification

Nils Erland L. Haugen[1] *Reginald E. Mitchell*[2] *Matt Tilghman*[2]

[1]*SINTEF Energy Research, Trondheim, Norway*

[2]*Department of mechanical engineering, Stanford University, USA*

In this work gasification of char is studied in a simulation code that includes a detailed 22 step heterogeneous reaction mechanism for char reactivity with CO_2, H_2O and O_2, and uses GRI-Mech 3.0 as the chemical kinetic mechanism that describes the impact of homogeneous reactions. The code is transient and zero dimensional in space, and is designed to be used both as a stand-alone gasification/combustion code and as a sub-model for heterogeneous reactions of solid particles in a CFD code both when the particle evolution is described by Lagrangian particle tracking and when an Eulerian-Eulerian methodology is chosen.
The main results for gasification of Wyodak coal char, in an environment similar to a full scale gasification reactor, are presented. It is shown that for many applications, it is important to account for inter-particle radiation, i.e. it is not sufficient to consider only radiative heat exchange between the particle and the surrounding wall, radiation between particles should be considered as well. Account is made for CO and H_2 inhibition in the model, and is shown to significantly affect char reactivity rates. The inhibition is due to CO or H_2 either blocking free carbon sites or reacting with adsorbed oxygen.

1 Introduction

There are three main routes to power production from coal with CO_2 capture and storage (CCS); pre-combustion, post-combustion and oxy fuel combustion. All three main routes have their advantages and disadvantages, and all of them will most likely be commercially used, but for different situations. For the pre-combustion route the gasification of coal to syngas is the ”heart” of the process. Coal gasification is also at the heart of a traditional IGCC plant, which in many respects is the starting point of a pre-combustion CCS plant.

The gasification process consists of the devolatilization phase, followed by the reaction of the volatiles and the char burnout phase. The char burnout proceeds through heterogeneous reactions between the gas and the solid phase. Single particle char burnout can be modeled using transient zero dimensional models, i.e. with no spatial discretization, which is done by e.g. Qiao et al. (2012) [1] and references therein. These zero dimensional models are fast and can potentially be used as sub-models for heterogeneous reactions in higher dimensional CFD tools.

For high reaction rates, i.e. when the diffusive time scale τ_D is much smaller than the reactive time scale τ_r such that the Damkohler number $\mathrm{Da} = \tau_D/\tau_r$ is much smaller than unity, the char particles will not be burning uniformly due to species gradients within the particles. In order to improve the

accuracy of the simulations one may then employ one dimensional models where radial gradients within the particles are resolved. This can be done both in a stationary [2] and a transient [3] fashion.

2 Equations

Let's define a volume V, enclosed by the surface S, containing a gas mixture with a constant number of N_p embedded char particles. Let the surface S be impermeable such that there is no mass flux over S and let it be flexible such that the volume V is allowed to change in order to keep the gas pressure of the enclosed gas constant. The total mass inside S is then constant and equal to $m = m_p N_p + m_g$ where m_p is the mass of each particle while m_g is the mass of the gas. It is clear that the gas density is given by $\rho_g = m_g/V$ while the particle number density is $n_p = N_p/V$.

Due to reactions between the gas phase and the particle phase there will be exchange of matter between the two phases. The change of the mass fractions of species i in the gas phase is correspondingly determined by the species production rate due to 1) the particle-to-gas reactions, $\omega_{pg,i}$, 2) the gas-to-gas reactions, $\omega_{gg,i}$, and 3) the gas-to-particle reactions, $\omega_{gp,i}$. For the char gasification we are interested in here the gas-to-particle reactions are insignificant and they will therefore be neglected them from now on.

The particle-to-gas reactions are determined by the set of reactions listed in Table 1. For this set of $N_{\text{reac,surf}} = 22$ heterogeneous reactions the generalized equation for surface adsorption and desorption due to reaction k is

$$\sum_{i=1}^{N_{\text{species}}} \nu_{i,k}\alpha_i + \sum_{j=1}^{N_{\text{ads}}} \mu_{j,k}\beta_j = \sum_{i=1}^{N_{\text{species}}} \nu'_{i,k}\alpha_i + \sum_{j=1}^{N_{\text{ads}}} \mu'_{j,k}\beta_j \tag{1}$$

where N_{species} is the number of gas phase species, N_{ads} is the number of adsorbed species and α_i and β_j represent gas phase species i and adsorbed solid phase species j, respectively. Furthermore $\mu_{j,k}$ and $\mu'_{j,k}$ are the stoichiometric coefficients of the adsorbed solid phase species on the reactant and product sides, respectively, while the stoichiometric coefficients of the gas phase species on the reactant and product sides are given by $\nu_{i,k}$ and $\nu'_{i,k}$, respectively.

2.1 Gas phase equations

The gas phase is described by three evolution equations. The mass equation

$$\frac{dm_g}{dt} = V \sum_{i=1}^{N_{\text{species}}} \omega_{pg,i} M_i, \tag{2}$$

where M_i is the molar mass of species i, allows for mass to be added to the gas phase due to reactions with the solid phase, while the species equation

$$\frac{dm_g Y_i}{dt} = V(\omega_{pg,i} + \omega_{gg,i})M_i, \tag{3}$$

Nr.	Reaction	A_k	$E_k/10^6$	$\sigma_k/10^6$	Dep. spec.
R1	$2C_f + H_2O \rightarrow C(OH) + C(H)$	9.20×10^{14}	105	0	H_2O
R2	$C(OH) + C(H) \rightarrow 2C_f + H_2O$	2.37×10^{12}	101	0	-
R3	$C(OH) + C_f \rightarrow C(O) + C(H)$	1.52×10^{14}	50	0	-
R4	$C(O) + C(H) \rightarrow C(OH) + C_f$	2.37×10^{14}	121	0	-
R5	$C(H) + C(H) \rightarrow 2C_f + H_2$	1.52×10^{12}	100	0	-
R6	$2C_f + H_2 \rightarrow C(H) + C(H)$	2.00×10^{14}	20	0	H_2
R7	$C(H) + C(OH) \rightarrow H_2 + C(O) + C_f$	1.52×10^{6}	155	0	-
R8	$C(O) + C_b \rightarrow CO + C_f$	1.00×10^{13}	353	28	-
R9	$C(H) + C_b \rightarrow CH + C_f$	1.00×10^{13}	433	36	-
R10	$C(OH) + C_b \rightarrow COH + C_f$	1.00×10^{13}	433	36	-
R11	$C(H) + C(H) \rightarrow CH_2 + C_f$	1.00×10^{9}	200	0	-
R12	$C_f + CO_2 \rightarrow C(O) + CO$	1.52×10^{7}	168	0	CO_2
R13	$C(O) + CO \rightarrow C_f + CO_2$	2.37×10^{5}	65.7	0	CO
R14	$C_b + C(O) + CO_2 \rightarrow C(O) + 2CO$	3.26×10^{16}	367	0	CO_2
R15	$C_f + CO \rightarrow C(CO)$	5.06×10^{4}	77.9	0	CO
R16	$C(CO) \rightarrow C_f + CO$	1.00×10^{13}	455	53	-
R17	$CO + C(CO) \rightarrow 2C_f + CO_2$	3.36×10^{9}	266	0	CO
R18	$2C_f + O_2 \rightarrow C(O) + CO$	6.50×10^{13}	102	0	O_2
R19	$2C_f + O_2 \rightarrow C_2(O_2)$	8.95×10^{9}	55	0	O_2
R20	$C_b + C_f + C(O) + O_2 \rightarrow C(O) + CO_2 + C_f$	1.18×10^{15}	120	0	O_2
R21	$C_b + C_f + C(O) + O_2 \rightarrow 2C(O) + CO$	3.74×10^{22}	227	0	O_2
R22	$C_b + C_2(O_2) \rightarrow 2C_f + CO_2.$	1.00×10^{13}	304	33	-

Table 1: Arrhenius parameters and dependent species for the surface reactions for Wyodak coal. The unit of both the activation energy E_k and the distribution width σ_k is J/kmol.

where Y_i is the mass fraction of species i, controls the total mass of any give species ($m_g Y_i$) in the gas phase. The total mass of a species changes either due to reactions in the gas phase itself or due to reactions between the gas and the solid phase. The energy equation can be expressed in the terms of enthalpy, h, as

$$\frac{d(m_g h)}{dt} = n_p V (Q_h + Q_c) \tag{4}$$

yielding that the enthalpy will change only due to heat Q_c or enthalpy Q_h being transferred from the solid phase to the gas phase.

The equation for the mass of the gas phase, (2), can be re-written as

$$\frac{dm_g}{dt} = \frac{m_g}{\rho_g} \sum_{i=1}^{N_{\text{species}}} \omega_{pg,i} M_i. \tag{5}$$

Using Eq. (5) it is also straight forward to re-write the species equation as

$$\rho_g \frac{dY_i}{dt} + Y_i \sum_{k=1}^{N_{\text{species}}} \omega_{pg,k} M_k = (\omega_{gg,i} + \omega_{pg,i}) M_i. \tag{6}$$

In order to find an equation for the temperature evolution one must use Eq. (3) to find

$$\begin{aligned}\frac{d(m_g h)}{dt} &= \sum_i \frac{d(m_g h_i Y_i)}{dt} = \sum_i m_g Y_i \frac{dh_i}{dt} + \sum_i h_i \frac{d(m_g Y_i)}{dt} \\ &= m_g c_{p,g} \frac{dT_g}{dt} + \sum_i h_i V(\omega_{pg,i} + \omega_{gg,i}) M_i \end{aligned} \quad (7)$$

where h_i is the enthalpy of species i, T_g is the temperature of the gas and where it has been utilized that the heat capacity of the mixture at constant pressure is $c_{p,g} = (\partial h/\partial T)_p$.

Combining Eq. (7) and Eq. (4) yields

$$\rho_g c_{p,g} \frac{dT_g}{dt} + \sum_{i=1}^{N_{\text{species}}} h_i(\omega_{gg,i} + \omega_{pg,i}) M_i = n_p(Q_h + Q_c). \quad (8)$$

The convective heat transfer between a particle and the gas is

$$Q_c = -H A_p (T_g - T_p) \quad (9)$$

when T_p is the temperature of the particle, $A_p = 4\pi r_p^2$ is the outer surface of the particle, r_p is its radius and the heat transfer coefficient can be expressed as [4]

$$H = \frac{\mathrm{Nu} k_g}{2 r_p} \frac{B}{\exp(B) - 1} \quad (10)$$

when Nu is the Nusselt number, k_g is the thermal conductivity of the gas mixture

$$B = \frac{\dot{m}_p c_{p,g}}{2\pi r_p \mathrm{Nu} k_g} \quad (11)$$

is the Stefan flow constant [5] and $\dot{m}_p = dm_p/dt$. Finally the enthalpy transfer between the particles and the gas is

$$Q_h = \sum_{i=1}^{N_{\text{species}}} \frac{\omega_{pg,i} h_i' M_i}{n_p}. \quad (12)$$

If the species i is a gaseous reactant the value of h_i' is evaluated at the temperature of the gas mixture while if it is a product of a solid phase reaction h_i' is evaluated at the particle temperature.

Furthermore the equation of state for a perfect gas is used;

$$P = \frac{\rho_g R T_g}{\overline{M}} \quad (13)$$

where the mean molar mass is

$$\overline{M} = \frac{1}{\sum_{i=1}^{N_{\text{species}}} Y_i / M_i}. \quad (14)$$

2.2 Particle phase equations

The evolution equation for the mass of the coal particle is given by

$$\frac{dm_c}{dt} = -S_t M_c \hat{R}_c \tag{15}$$

when $S_t = S_{gc} m_c$ is the total surface area of the particle, M_c is the molar mass of coal, $\hat{R}_c$ is the molar reaction rate of coal and S_{gc} is the specific surface area of the particle. In the current work we have used $S_{gc,0} = 3 \times 10^5$ m^2/kg, which is a valid number for sub-bituminous coal. Since $R_i = \hat{R}_i M_i$, Eq. (15) can be re-written to read

$$\frac{1}{m_c}\frac{dm_c}{dt} = \frac{\dot{m}_c}{m_c} = -S_{gc}\hat{R}_c \tag{16}$$

when $\dot{m}_c$ is the carbon consumption rate due to heterogeneous reactions. The total surface are of a particle was found by [6] to be

$$S_t = (1-x)S_{t,0}\sqrt{1-\psi\ln(1-x)} \tag{17}$$

for zone I combustion when the carbon conversion x is

$$x = 1 - \frac{m_c}{m_{c,0}}. \tag{18}$$

A more general expression, which in addition to zone I also allows for zone II and III combustion, is presented by [3];

$$S_t = (1-x)S_{t,0}\sqrt{1-\psi\ln\left(\frac{\rho_c}{\rho_{c,0}}\right)} \tag{19}$$

which should be valid for all zones and reduce to the expression of [6] for zone I combustion.

The particle temperature equation is given by

$$\frac{dT_p}{dt} = \frac{1}{m_p c_{p,p}}\left(Q_{\text{reac}} - Q_c + Q_{\text{rad}}\right) \tag{20}$$

when $c_{p,p}$ is the specific heat capacity of carbon.

The net heat of reaction of the particle due to solid phase reactions is

$$Q_{\text{reac}} = \sum_{k=1}^{N_{\text{reac,surf}}} \dot{m}_{c,k} q_{\text{reac},k} \tag{21}$$

when $N_{\text{reac,surf}}$ is the number of heterogeneous reactions and $q_{\text{reac},k}$ is the heat of reaction for surface reaction k. The molar heat of reaction for reaction k is given by

$$\hat{q}_{\text{reac},k} = \sum_{i=1}^{N_{\text{surf,spec}}} \nu_{i,k} h_i - \nu'_{i,k} h_i + \sum_{j=1}^{N_{\text{ads}}} \mu_{j,k} h_j - \mu'_{j,k} h_j \tag{22}$$

when h_i is the enthalpy of formation of species i. The enthalpy of formation of the adsorbed species, h_j, has in the current work been set to half the value of the corresponding non-adsorbed species. It is found that the final result is not very sensitive to the method used to find h_j and it is therefore believed that the errors introduced due to the lack of knowledge of the exact value of h_j are minor.

The radiative heat from the particle to the wall is traditionally described as

$$Q_{\rm rad} = 4\epsilon\sigma\pi r_p^2(T_w^4 - T_p^4) \tag{23}$$

where ϵ, σ and T_w is the emissivity, Stefan-Boltzmann constant and the wall temperature, respectively. Here gas phase radiation and radiation between particles have been neglected.

When accounting for inter particle radiation, and picking the average particle within the enclosure, the radiative term can be shown to be

$$Q_{\rm rad} = \frac{3f(\beta)\sigma}{n_p R}(T_w^4 - T_p^4) \tag{24}$$

where

$$f(\beta) = 1 - \frac{1}{2\beta^2} + e^{-2\beta}\left(\frac{1}{\beta} + \frac{1}{2\beta^2}\right) \tag{25}$$

the optical depth is $\beta = aR$, R is the radius of the enclosure and $a = \pi r_p^2 n_p$ is the absorption coefficient due to the particles. In the above the average particle is defined such that $Q_{\rm rad} n_p V = E_{\rm wall,net}$ where $E_{\rm wall,net}$ is the net radiation to the wall.

The Sherwood number

$$\mathrm{Sh} = \frac{2r_p k_{im}}{C_g D_{im}} \tag{26}$$

is set to two since the Reynolds number is assumed to be negligible. From the above equation the mass transfer coefficient is found to be

$$k_{im} = \frac{C_g D_{im}}{r_p} \tag{27}$$

when D_{im} is the molecular bulk diffusivity of species i and the total gas concentration is

$$C_g = \frac{\rho}{\overline{M}} = \frac{P}{RT_p}. \tag{28}$$

Given a rate for reaction k, $\hat{RR}_k$, the production rate of carbon per total particle surface area is

$$R_{c,k} = M_c \sum_{i=1}^{N_{\rm species}} \hat{RR}_k(\nu'_{i,k} - \nu_{i,k})a_{c,i} \tag{29}$$

when $a_{c,i}$ is the number of carbon atoms in species i. From Eq. (16) it can be seen that the carbon consumption rate due to reaction k may be written as

$$\dot{m}_{c,k} = -S_t R_{c,k}. \tag{30}$$

Furthermore, the molar production rate per particle outer surface area of species i from reaction k is

$$\dot{n}_{i,k} = (\nu'_{i,k} - \nu_{i,k})\hat{RR}_k \frac{S_t}{A_p}. \tag{31}$$

2.3 Absorbed species

We now want to look at species adsorbed to the particle surface; the number of kmoles of species j on the particle surface is given by

$$N_j = C_{s,j} S_t \tag{32}$$

when $C_{s,j}$ is the concentration of species j on the surface. This yields

$$\frac{dN_j}{dt} = \frac{dC_{s,j}}{dt} S_t + C_{s,j} \frac{dS_t}{dt} \tag{33}$$

which can be expressed in terms of the evolution of the concentration as

$$\frac{dC_{s,j}}{dt} = \frac{1}{S_t} \frac{dN_j}{dt} - \frac{C_{s,j}}{S_t} \frac{dS_t}{dt}. \tag{34}$$

It is clear that

$$\frac{dN_j}{dt} = \hat{R}_j S_t \tag{35}$$

when $\hat{R}_j$ is the molar production rate of adsorbed species j (see Eq. (50)) such that

$$\frac{dC_{s,j}}{dt} = \hat{R}_j - \frac{C_{s,j}}{S_t} \frac{dS_t}{dt}. \tag{36}$$

The site fraction of species j is

$$\Theta_j = \frac{C_{s,j}}{\xi_n} \tag{37}$$

where ξ_n is the total surface concentration of all carbon sites, whether occupied or not. This means that

$$\sum_{j=1}^{N_{\text{ads}}} \Theta_j = 1, \tag{38}$$

when N_{ads} is the total number of occupying species and the free carbon sites are counted as a species. From Eq. (36) it follows that

$$\frac{d\Theta_j}{dt} = \frac{\hat{R}_j}{\xi_n} - \frac{\Theta_j}{S_t} \frac{dS_t}{dt}. \tag{39}$$

By using Eqs. (16) and (18), assuming zone 1 combustion and differentiating Eq. (19) it is found that the evolution of the total surface area is given by

$$\frac{1}{S_t} \frac{dS_t}{dt} = \left(\frac{S_{t,0}^2 \psi \left(1-x\right)^2}{2 S_t^2} - 1 \right) S_{gc} M_c \hat{R}_c = -A \hat{R}_c \tag{40}$$

when

$$A = \left(1 - \frac{S_{t,0}^2 \psi \left(1-x\right)^2}{2 S_t^2} \right) S_{gc} M_c \tag{41}$$

such that from Eq. (39) and Eq. (40) the evolution equation for the site fractions of species i is

$$\frac{d\Theta_j}{dt} = \frac{\hat{R}_j}{\xi_n} + A\hat{R}_c\Theta_j. \tag{42}$$

One must now solve the evolution equation for the site fraction of each of the adsorbed species, the only exception is for the free carbon sites, Θ_{cf}, which are found from

$$\Theta_{cf} = 1 - \sum_{i \neq cf} \Theta_i. \tag{43}$$

2.4 Species concentrations at the particle surface

The molar flux of each gaseous species i at the particle surface can be expressed as

$$\dot{n}_i = \sum_{k=1}^{N_{\text{reac,surf}}} \dot{n}_{i,k} \tag{44}$$

when $\dot{n}_i$ is given by Eq. (31). The production rate of species i due to surface reactions is then

$$\omega_{pg,i} = \dot{n}_i A_p n_p. \tag{45}$$

By assuming steady state for the volume fraction of the species at the particle surface, $X_{i,s}$, is given by

$$\dot{n}_i - X_{i,s}\dot{n}_{\text{total}} = -k_{im}(X_{i,\infty} - X_{i,s}) \tag{46}$$

which is solved by using the Newton-Raphson method to find the root of

$$f_i(X_{i,s}) = X_{i,s} - \frac{k_{im}X_{i,\infty} + \dot{n}_i}{k_{im} + \dot{n}_{\text{total}}} \tag{47}$$

when $\dot{n}_{\text{total}} = \sum_i \dot{n}_i$. The second term on the left hand side of Eq. (46) is due to the Stefan flow. For infinitely fast mass diffusion this equation simplifies to $X_{i,s} = X_{i,\infty}$ which can be used for testing the simulation code.

It turns out that for very early times a steady state solution to the species surface mole fractions may not exist, yielding unphysical values. It has therefore been decided to solve the time dependent equation for the surface species mole fractions instead;

$$\frac{dX_{i,s}}{dt} = \frac{A_p}{\theta C_g V_p}\left(\dot{n}_i - \dot{n}_{\text{total}}X_{i,s} + k_{im}(X_{i,\infty} - X_{i,s})\right). \tag{48}$$

This explicit equation yields almost exactly the same results as the implicit method except at very early times and it is much more stable and robust.

2.5 Surface reactions

The rate expression of sub reaction k is given by

$$\hat{RR}_k = k_k \left(\prod_{j=1}^{N_{\text{ads}}} C_{s,j}^{\mu_{j,k}} \right) \left(\prod_{i=1}^{N_{\text{species}}} C_{g,i}^{\nu_{i,k}} \right) \tag{49}$$

when k_i is the rate coefficient and $C_{g,i} = C_g X_{i,s}$. The molar production rate of adsorbed species j is

$$\hat{R}_j = \sum_{k=1}^{N_{\text{surf,reac}}} (\mu'_{j,k} - \mu_{j,k}) \hat{RR}_k. \tag{50}$$

The rate constant for each of the sub reactions is given by

$$k_k = A_k \exp(-E_k/(RT)) \tag{51}$$

where the values of A_k and E_k for each sub reaction is found in Table 1.

For reactions R8, R9, R10, R16 and R22 there is a distribution of activation energies such that

$$k_k = \int_0^\infty k_k(E) f(E) dE \tag{52}$$

where

$$f(E) = \frac{1}{\sigma\sqrt{2\pi}} \exp\left[-\frac{1}{2} \left(\frac{E - E_k}{\sigma} \right)^2 \right]. \tag{53}$$

Eq. (52) is solved numerically using 20 numerical bins and integrating from $E_k - 6\sigma_k$ to $E_k + 6\sigma_k$.

2.6 Internal particle burning and the effectiveness factor

It is customary to think of a porous char particle as being composed of a large number of small pores in which the gas phase species diffuse. For large pores, i.e. when the pore diameter d_p is significantly larger than the mean free path λ of the gas phase molecules, the pore diffusion is described by the usual bulk diffusion of the molecules. If, however, the pore diameter is much smaller than the mean free path, the molecules will typically not collide with other molecules but rather with the pore wall. This is referred to as Knudsen diffusion. The Knudsen diffusion for species i is given by

$$D_{\text{K},i} = \frac{2 r_{\text{pore}} \theta}{3\tau} \sqrt{\frac{8RT_p}{\pi M_i}} \tag{54}$$

where τ is the tortousity factor, which here is set to 3, introduced in order to account for the fact that the pores are not purely in the radial direction and $r_{\text{pore}} = 2 f_r \theta / (\rho_p S_{gc}) = 2 f_r \theta V_p / S_t$ is the mean pore radius, V_p is the particle volume and f_r is the roughness factor, which is set to 2 [7]. The porosity of the char particle is given by $\theta = 1 - \rho_p / \rho_{c,t}$ where ρ_p is the apparent density of the particle and $\rho_{c,t} = 1.8$ kg/m^3 is the true density of carbon.

When calculating the effective diffusion $D_{\text{eff},i}$ through the particle pores account must be made for the combined effect of bulk diffusion and Knudsen diffusion. The importance of the Knudsen

diffusion is determined by the Knudsen number $\mathrm{Kn} = \lambda/d_p$ which is a measure of how important molecule collisions with the pore wall is compared to inter molecule collisions. Knowing both the bulk and the Knudsen diffusion coefficients the effective diffusion coefficient of species i is given by

$$\frac{1}{D_{\mathrm{eff},i}} = \frac{1}{D_i} + \frac{1}{D_{\mathrm{K},i}}. \tag{55}$$

If the mass diffusion within the particle is slow compared to the heterogeneous reactions it is clear that the reactant concentration will not be homogeneous throughout the particle. The total particle reaction rate will then be lower than expected. This reduction in reaction rate is given by the effectiveness factor

$$\eta_i = \frac{\text{Actual overall reaction rate of reactant species } i}{\text{Maximum possible reaction rate of reactant species } i} \tag{56}$$

and it was found by Thiele [8] that this could be expressed as

$$\eta_i = \frac{3}{\phi_i}\left[\frac{1}{\tanh(\phi_i)} - \frac{1}{\phi_i}\right] \tag{57}$$

where the Thiele modulus is

$$\phi_i = r_p\sqrt{\frac{\hat{R}_i \rho_p S_{gc}}{C_g X_i D_{\mathrm{eff,i}}}}. \tag{58}$$

For an n'th order reaction this has later been found to be

$$\eta_i = \frac{3}{\phi_{n,i}}\left[\frac{1}{\tanh(\phi_{n,i})} - \frac{1}{\phi_{n,i}}\right] \tag{59}$$

where

$$\phi_{n,i} = \phi_i\sqrt{(n+1)/2}. \tag{60}$$

Subscript i refers to the reactant of the reaction which could be e.g. O_2, H_2O or any other reactant species. Different reactions may have different reactants and one must then use the correct Thiele modulus to find the effectiveness factor of that reaction. The molar reaction rate of reactant i is given by

$$\hat{R}_i = \sum_{k=1}^{N_{\mathrm{surf,reac}}} (\nu'_{i,k} - \nu_{i,k})\hat{RR}_k. \tag{61}$$

The reaction rates given by Eq. (49) is now augmented to read

$$\hat{RR}_k = \eta_k k_k \left(\prod_{j=1}^{N_{\mathrm{ads}}} C_{s,j}^{\mu_{j,k}}\right)\left(\prod_{i=1}^{N_{\mathrm{species}}} C_{g,i}^{\nu_{i,k}}\right) \tag{62}$$

where η_k is the effectiveness factor of reaction k, which equals the effectiveness factor for the dependent gas phase species of reaction k. The dependent gas phase species for each reaction is listed in the last column of Table 1. If reaction k does not have a dependent species the effectiveness factor is set to one.

2.7 Burning mode

The mode of burning, i.e. the relation between particle radius, density and mass is straight forward for zone 1 and zone 3 burning. Generally, however, one can say that for the times t and $t + \delta t$ the particle mass and density are related as

$$\frac{\rho_{p,t+\delta t}}{\rho_{p,t}} = \left(\frac{m_{p,t+\delta t}}{m_{p,t}} \right)^{\alpha} \tag{63}$$

while the rationship between the particle mass and radius is given by

$$\frac{r_{p,t+\delta t}}{r_{p,t}} = \left(\frac{m_{p,t+\delta t}}{m_{p,t}} \right)^{\beta} \tag{64}$$

such that $\alpha = 1$ for zone 1 burning and $\alpha = 0$ for zone 3. In the previous equation superscript t and $t + \delta t$ refers to the values at times t and $t + \delta t$, respectively. Furthermore, by assuming spherical particles, it can be found that $\alpha + 3\beta = 1$. Since, as already stated, $\alpha = 1$ for zone 1 burning when the particle is totally penetrated by the reactive gases and the effectiveness factor is one, and α approaces zero for zone 3 burning when the reactions only occur at the outer surface of the particle such that the effectiveness factor approach zero, it seems reasonable to equate α with the mean effectiveness factor, i.e.

$$\alpha = \overline{\eta} \tag{65}$$

in order to close the equation.

3 Results

The test cases reported in the following have conditions similar to a typical entrained flow gasifier operating at 24 bar and a temperature of 1640 K. See Table 2 for more properties of the base case.

Property	Symbol	Value	Unit
Surf. conc. of C sites	ξ	1.08×10^{-7}	kmol/m^2
Spec. init. part. surf. area	$S_{gc,0}$	3×10^5	m^2/kg
App. density of part.	ρ_p	1300	kg
Particle radius	r_p	5×10^{-5}	m
Pressure	P	24	Bar
Initial temperature	T_{in}	1640	K
Mole fraction O_2	X_{O_2}	0.73	-
Mole fraction N_2	X_{N_2}	0.14	-
Mole fraction H_2O	X_{H_2O}	0.13	-
Carbon to gas mass ratio	m_p/m_g	0.65	-
Mean molar mass	$\bar{M}$	29.6	kg/kmol
Initial gas density	ρ_g	5.3	kg/m^3

Table 2: Properties of a typically entrained flow gasifier, used as the initial conditions for the base case.

In the left hand panel of Fig. 1 the char conversion is shown as a function of time for different cases. First of all it should be noted that the initial increase in conversion is very fast, before it slows down from a conversion of around 0.8. For the base case, 78% of the total time used to reach full conversion is spend gasifying only the last 20% of the particle mass. This feature will be explained later. In the right hand panel of Fig. 1 the particle and gas phase temperatures are

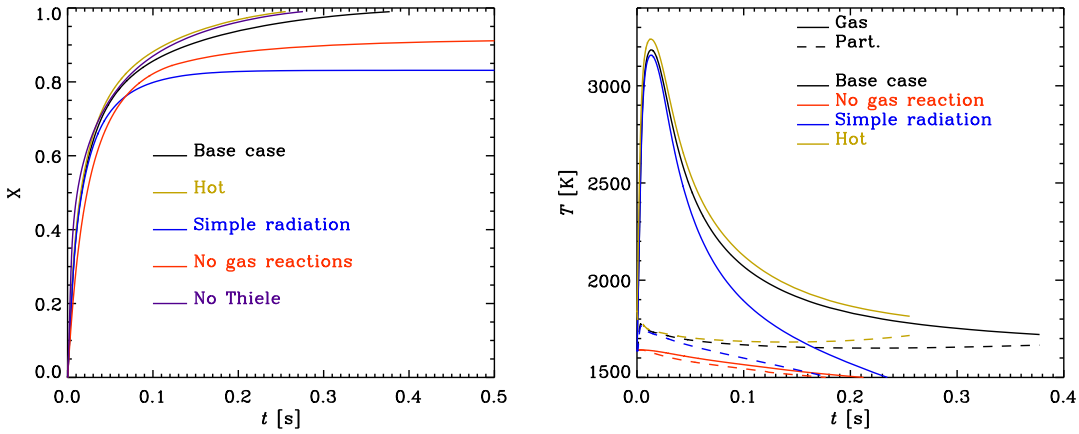

Figure 1: Particle and gas phase temperatures (right) and carbon conversion (left).

shown as a function of time. It may be surprising to see the very high gas phase temperature for the base case at intermediate times, but this is due to gas phase reactions as can be seen by comparing the base case and the case without gas phase reactions (red line). Even though the gas phase temperature goes up to above 3000 K it is down to around 1800 K at the end of the gasification process. This temperature is less than 200 K above the initial temperature. The very high gas phase temperature does not have much impact on the particle temperature as it is relatively constant and always below 1800 K. For the blue line the traditional radiation expression, given by Eq. (23), is used, while for all the other lines the expression given in Eq. (24) is used for the radiation. Since the traditional radiation expression does not take into account the radiative heating from all the surrounding particles it yields too strong cooling for full scale gasification reactors. The temperature evolution for the black and the blue lines are very similar at early times, but at later times the blue line, with the simplified radiation expression, naturally shows the effect of the stronger cooling. The radiative cooling is actually so strong that full conversion is not reached before the chemical reactions are quenched due to the low temperatures.

Increasing the initial gas and particle temperatures by 200 K gives a somewhat reduced gasification time as can be seen from the yellow/green line in Fig. 1. Even though both the gas and particle temperatures were initially 200 K higher than for the base case it can be seen that for almost all the time spent gasifying the particle the temperature difference between the two cases is less than 50 K.

The gas phase temperature and composition at the end (99% conversion) of the base case simulation are listed in Table 3 under the column named “End sim.”. In order to check if the mixture is in equilibrium at the end of the simulation the condition at the end of the simulation is fed into an equilibrium solver and the results are shown in the same table for constant enthalpy and pressure

	End sim.	Equi. (HP)	Equi. (TP)
T [K]	1721.	1585.	1721.
CO	0.67731	0.69112	0.69280
H2	0.19622	0.24474	0.24385
H2O	0.03785	0.02032	0.02175
CO2	0.03737	0.01951	0.01767
N2	0.02503	0.02376	0.02375
CH4	0.01849	0.00049	0.00012
C2H2	0.00638	0.00000	0.00000
C2H4	0.00126	0.00000	0.00000
HCN	0.00002	0.00004	0.00003
SUM	0.99991	0.99997	0.99996

Table 3: Temperature and species mole fractions of the gas phase at the end of the simulation (End sim.) compared to equilibrium values. The equilibrium values are calculated from the condition at the end of the simulation, assuming adiabaticity (Equi. (HP)) or constant temperature (Equi. (TP)).

(Equi. (HP)) and for constant temperature and pressure (Equi. (TP)). It is clear that even though gas phase reactions are fast at these temperatures the gas phase mixture is not in equilibrium at the end of the simulation. In particular the concentrations of H_2O and CO_2 are around a factor 2 too high, while the concentrations of CH_4, C_2H_2 and C_2H_4 are orders of magnitude too high.

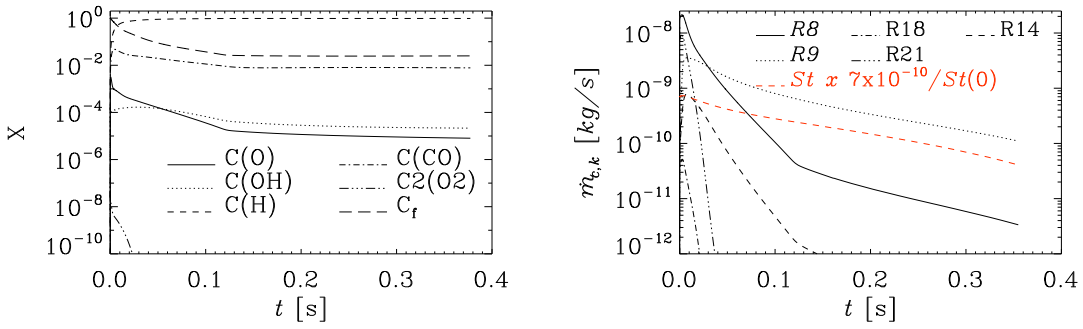

Figure 2: Coverage fraction of the adsorbed species (left panel) and carbon conversion rate for different reactions (right panel).

In figure Fig. 1 it was shown that the char particle reaction rate flattens out, yielding an almost constant change in conversion, from $t \sim 0.13$. In Fig. 2 (left panel) this is shown to be due to the coverage fraction of adsorbed species being essentially constant after $t = 0.12$. The coverage fraction of adsorbed H is very high, almost one, and is effectively inhibiting the reactions since it yields a coverage fraction of free carbon sites as low as $\sim 3 \times 10^{-2}$.

In the right panel of figure Fig. 2 the carbon conversion rate as a function of time is shown for the most important reactions. Traditionally reaction R8 ($C(O) + C_b \rightarrow CO + C_f$) is thought to be the dominant one for carbon conversion but here it is seen that only for early times is R8 larger than R9 ($C(H) + C_b \rightarrow CH + C_f$). This is clearly due to the amount of adsorbed H being around 5 orders of magnitude larger than the amount of adsorbed O. When looking more carefully at the

data it becomes clear that since the carbon conversion is so much faster in the initial phase of the simulation most of the carbon conversion is still due to reaction R8, as expected.

The red dashed line in the right hand panel of Fig. 2 shows $S_t e/S_{t,0}$ and from this is is clear that the reason for the decrease in carbon conversion due to R9 is simply due to the reduction in total particle surface area S_t. This is as expected since the temperature and coverage fraction of C(H) are essentially constant for late times. In the above e is just a plotting constant and has now physical meaning. It can also be seen that adsorbed CO block some amount of free sites, but this is not as important as the adsorbed H.

In Fig. 3 it is seen that the hydrogen in the ambient is not inhibiting the reactions directly since the reaction rate $\hat{RR}_6 - \hat{RR}_5$ is negative most of the time, i.e. adsorbed H ultimately comes from reactions with H_2O and not from reactions with H_2. The hydrogen in the ambient does however inhibit the reactions indirectly since they increase the importance of R6 compared to R5 making $\hat{RR}_6 - \hat{RR}_5$ less negative than it would otherwise be.

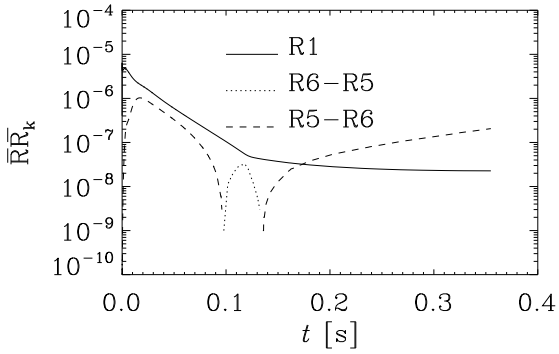

Figure 3: Here is shown $\hat{RR}_1$ (solid line), $\hat{RR}_6 - \hat{RR}_5$ (dotted line) and $\hat{RR}_5 - \hat{RR}_6$ (dashed line).

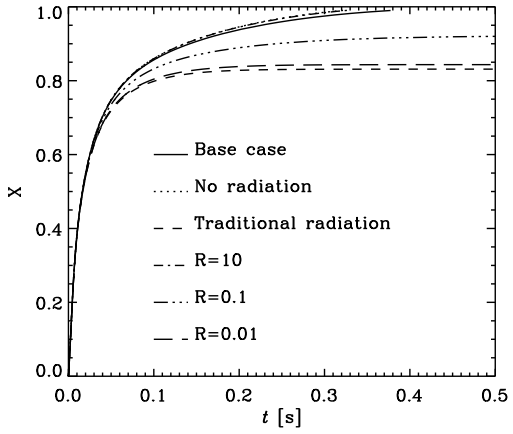

Figure 4: Conversion as a function of time for various treatments of the radiation.

In Fig. 4 the conversion as a function of time for simulations with different enclosure sizes are shown together with a simulation without any radiation model and a simulation with the tradi-

tional radiation model (Eq. (23)). For all these simulations the particle number density, n_p, is kept constant such that the absorption coefficient is also constant. This means that when the enclosure size is increase so is also the optical thickness. It can be seen that as expected the simulation with traditional radiation yields the slowest conversion, and as mentioned previously, ultimately does not even convert all the carbon due to too low temperatures. The enclosure with radius $R = 0.01$ m yield results very similar to the case with traditional radiation since the optical depth in this case is very low such that inter particle radiation is small compared to particle wall radiation. Increasing the domain size to $R = 0.1$ m gives some more conversion, but even here full conversion is not reached. Finally the case with $R = 10$ m, being very optically thick, give results very similar to the case without any radiative cooling at all. This is reasonable since the fraction of particles "seeing" the cold wall is very small. The base case, having $R = 1$ m, also being relatively optically thick, lays very close to the case without radiation.

4 Conclusion

Single particle gasification is simulated with a high fidelity zero dimensional simulation tool. Results are shown for different simulations meant to represent conditions of a typical entrained flow gasifier. The amount of adsorbed H in particular, but also to some extent the amount of adsorbed CO, is found to severely block the available free carbon sites. This yields a very low reaction rate for conversions larger than about 80%. The high fraction of adsorbed H is not directly due to adsorption of H_2 from the ambient, but indirectly due to the large fraction of H_2 shifting the equilibrium in the H_2 adsorption-desorption towards less desorption.

The effect of different radiation models and the size of the gasification environment is investigated. It is found that the traditional radiation model neglecting inter particle radiation is applicable only for very small enclosures. For enclosures of dimensions of one meter and up it is actually more accurate to neglect radiation all together than to use a radiation model which neglects inter particle radiation.

Acknowledgments

NELH acknowledges The Norwegian Research Council for its support through the CAMPS project.

References

[1] L. Qiao, J. Xu, A. Sane and J. Gore, Combustion and Flame **159**, 1693 (2012).

[2] E. S. Hecht, C. R. Shaddix, A. Molina and B. S. Haynes, Proceedings of the combustion institute **33**, 1699 (2011).

[3] R. E. Mitchell, L. Ma and B-J Kim, Combustion and Flame **151**, 426 (2007).

[4] Y. C. Guo, C. K. Chan and K. S. Lau, Fuel **82**, 893 (2003).

[5] D. A. Frank-Kamenetskii, *Diffusion and heat transfer in Chemical Kinetics*. Plenum Press, New York (1969).

[6] S. K. Bhatia and D. D. Perlmutter, AIChE J. **26**, 379 (1980).

[7] A. Wheeler, Advances in Catalysis **3**, 249 (1951).

[8] E. W. Thiele, Ind. Eng. Chem **31**, 916 (1939).